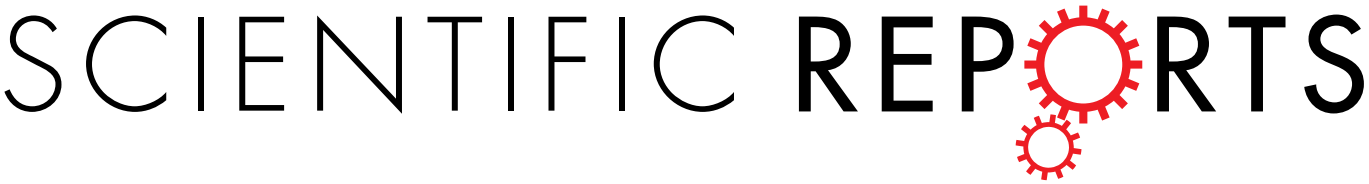

OPEN

Non quasi-Hemispherical Seismological Pattern of the Earth's Uppermost Inner Core

Received: 28 July 2017
Accepted: 18 January 2018
Published online: 02 February 2018

Marian Ivan[1], Rongjiang Wang[2] & Rami Hofstetter[3]

We assembled a database consisting of 5,404 PKIKP/PKiKP observations from 555 events, where PKIKP is the phase sampling the inner core (IC) and PKiKP is the phase reflected at the inner core boundary (ICB). Around 138° distances, their differential arrival times and amplitude ratio are mostly sensitive to the seismic velocity and attenuation structure in the uppermost IC (UIC), respectively. Our observations do not support a large-scale anisotropy in the UIC, but do not exclude its presence in some restricted areas. A robust inversion for the isotropic P-wave velocity perturbations shows a higher velocity cap with a radius of ~60°, approximately centered beneath the Northern Sumatra, with a local low velocity zone beneath the central Indian Ocean. The rest of the UIC, including the Northern part of Eurasia and of the Atlantic Ocean, exhibits mostly lower velocity. Amplitude ratio values of PKIKIP/PKiKP (observed vs. computed) from 548 high signal-to-noise (>5) recordings show a large variance, suggesting only a faint correlation between higher velocity and lower attenuation in the UIC. Our results provide better constraints to the models invoking a heat transfer in the UIC, with a complex temperature pattern near ICB.

The internal structure and composition of the Earth's inner core (IC) provides realistic conditions for the geodynamo and is essential for the understanding of the outer core (OC) and of the mantle dynamics[1]. Therefore, it is important to accurately map the spatial distribution of P-wave velocity and attenuation, especially in the uppermost IC (UIC, roughly the top 100 km beneath the IC boundary). Seismological evidence suggests a quasi-hemispherical dichotomy of the UIC[2,3], with a meridian separation. It is considered that the quasi-Eastern hemisphere (qEH, commonly assumed from 40° E to 180° E) displays a higher velocity (and lower attenuation) with respect to a 1-D global reference model. The opposite situation is assumed for the quasi-Western hemisphere (qWH, from 180° W to 40° E). Various other studies obtained slightly different boundaries between the two q-Hs, with possible variations of the above limits with depth[4,5]. Anisotropy in the UIC is also questionable, from an isotropic or weakly anisotropic UIC[3,6–8], (especially in the qEH), to complex models involving the variation of anisotropy and/or attenuation with depth at the top of the IC[9–11]. Yet, the results related to the UIC anisotropy beneath Africa[9] are obtained near a presumed boundary of the two q-Hs, where heterogeneity is routinely difficult to separate from anisotropy.

Attempts to link the available seismological observations to thermal effects near the ICB also considered a (quasi)-hemispherical IC[12]. Differential arrival times of phases with similar path in the mantle are routinely assumed to be related to the lateral variations of waves' velocity in the proximity of ICB and/or to irregularities of ICB topography[13]. Such disturbances with respect to a 1-D global reference model are assumed to be an effect of the lateral variations in temperature or composition of the UIC, but the exact relation chemistry, freezing (or melting) and the velocity/attenuation /topography perturbations cannot be resolved directly by seismological observations[14]. For example, a convection model of the inner core[1,12] predicts freezing in the qWH, centered at G (growth) point around (0, 80°W), and melting in the qEH (around M point, near (0, 100°E). Alternatively, heat is extracted from the outer core by the vigorous mantle convection, large enough to allow heat flowing into the inner core[15,16]. In such a model, freezing is dominant in the qEH, while a large zone of melting is located in the qWH. At least in some areas, a correlation between the core-mantle velocity pattern and the ICB one is expected. Some thermal models[12] require (at least) a degree one spherical harmonic pattern, as described by a (linear) variation in cos(Δ) (where Δ is the angular distance of the PKIKP bouncing point to a certain cold or warm pole). While

[1]University of Bucharest, Bucharest, Romania. [2]Helmholtz Center Potsdam, GFZ German Research Center for Geosciences, Potsdam, Germany. [3]Geophysical Institute of Israel, Lod, Israel. Correspondence and requests for materials should be addressed to M.I. (email: marian.ivan@g.unibuc.ro)

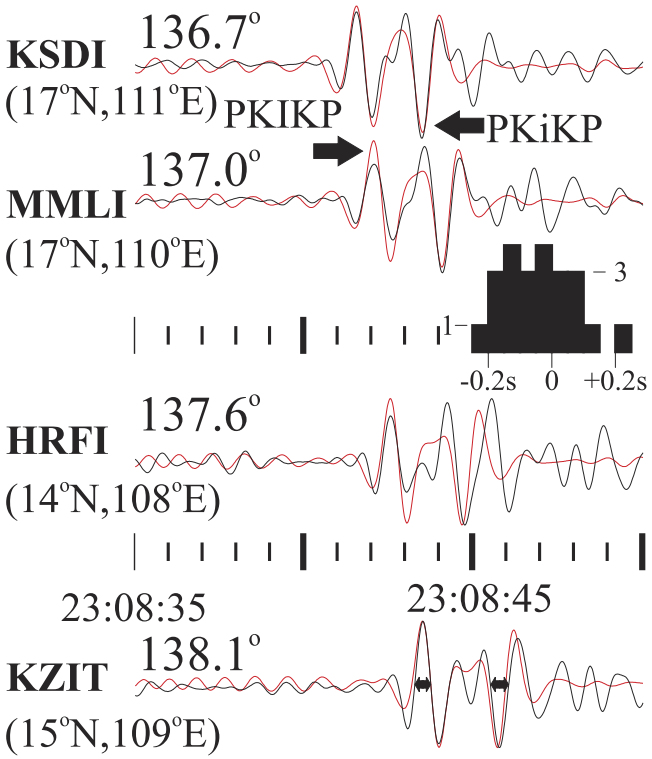

Figure 1. Recordings at some Israel Seismic Network stations of 2013, April, 13th Vanuatu event. A zero-phase Butterworth band-pass filter in the range 0.7 to 2 Hz has been applied both to the broad-band vertical recordings (black) and to the corresponding synthetics (red). Epicentral distances are shown. The location of the PKIKP bouncing points (indicated in the parenthesis) is in the very proximity of the central meridian (110°E longitude) of the quasi-Eastern Hemisphere. Yet, all the differential times are very close to zero. The inset histogram is obtained for the 23 differential times at the stations in Turkey for the same earthquake, and for the 2017, April, 5th Vanuatu event. The bouncing points are in the same area. The mean of the differential times is −0.05 +/− 0.05 seconds (95% confidence error), significantly different from a value of 0.65 seconds obtained from a velocity perturbation around 1% (in respect to ak135 model) as suggested from the q-EH model[49]. The time windows used to obtain the differential times at KZIT station are approximately indicated by the double horizontal arrows.

some observations[12] show a linear variation in Δ only, other data sets[17] suggested a sharp transition between the two qHs, compatible with models of a translating inner core[18].

Recently, some local departures from a longitude line separation between the two q-Hs have been reported, challenging the q-H pattern for the deeper part of the core[5,11,19–23]. To accurately identify their spatial position, a proper knowledge of the velocity pattern in the UIC is needed as well.

Data and preliminary processing

To explain some of the above discrepancies, we analyzed a large data set of high quality PKIKP/PKiKP global observations from 553 earthquakes and two nuclear explosions (1993, October, 5th and 1996, January, 27th). We select mostly intermediate to deep depth events to minimize signal disturbances by the depth phases and short-period scattering effects. Some good recordings from shallow earthquakes are also used, but carefully examined to avoid misinterpretation of the PKiKP by PKIKP depth phases. Earthquakes with a complex source-time function are discarded. The entire list of events can be found as Supplementary Table S1. The observations are made in the distance range 133°–142°. At shorter distances, the arrival times of the two phases are too close to each other. At greater distances, the signal is usually severely disturbed by the high amplitude of the short-period precursors (PKPpre, or PKhKP) anticipating the PKIKP arrival, due to the increasing amplitude of PKP_Bdif near B-caustic point around 145°.

Synthetic seismograms are used as reference, calculated using the code QSSP[24] based on the ak135 global Earth model and Global Centroid Moment Tensor source parameters[25,26]. If available, the earthquake locations are taken preferably from the ISC Bulletin[27,28]. Some examples of recorded and synthetic core phases are shown in Fig. 1. The differential times are estimated by cross correlation between the recorded or synthetic phases for time windows of ~0.5 s length, starting immediately following the wave onset on the broad-band, vertical recording. A zero-phase Butterworth band-pass filter in the range 0.7 Hz–2 Hz has been applied[29], to the recordings and synthetics. We estimate the accuracy in the evaluation of PKiKP vs. PKIKP (O-C, observed minus computed) to be better than 0.1 seconds. This accuracy estimation is supported by the estimations made at a large number of

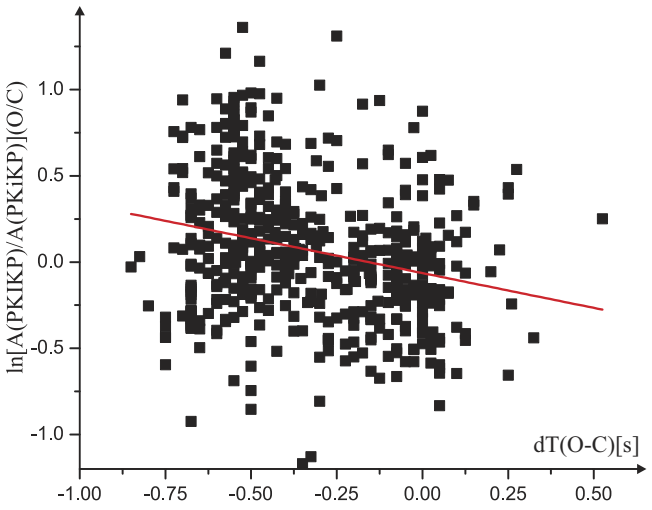

Figure 2. Natural logarithm of the amplitude ratio values of PKIKP/PKiKP (Observed/Computed) vs. the differential times from 548 high (>5) signal-to-noise observations. R-square value of the linear regression is equal to 0.08, indicating a large variance in the data (R-squared = 1 for a linear correlation).

highly confined stations from the same array or local network. The PKIKP phases recorded at these stations are sampling almost the same region of the IC.

Amplitudes of both PKIKP and PKiKP might be disturbed if short-period precursors are significant in the recordings. We select 548 recordings with the PKIKP at least five times larger than the maximum amplitude of the forerunners observed in a 12 second time window anticipating the PKIKP onset. The amplitude ratios values of PKIKP/PKiKP (Observed/Computed) show a large variance, in many cases observed for stations of the same array or local network (Fig. 2). For example, 19 observations at the Warramunga array of the 2007, September 26th Ecuador event provided an average differential time of −0.44 +/− 0.03 seconds (95% confidence error) and an average natural logarithm (NL) of the amplitude ratio equal to 0.09 +/− 0.08. The PKIKP paths sampled the UIC in the Southern Pacific. In the case of the 2017, June, 24th South Peru event, 22 observations at the same array show −0.54 +/− 0.02 seconds for the differential time, but 0.76 +/− 0.05 for the NL amplitude ratio. Similar variance of the amplitude ratio (or even greater) is routinely observed at stations in Kazakhstan but also at the GRF and YKA arrays. It indicates that IC regions with much closed velocity values may show large variance in attenuation. In particular, 18 observations at the Central Asia stations BRVK, BVAR, CHKZ and VOS from 12 South Sandwich earthquakes show the differential times close to zero (a mean value of 0.02 +/− 0.04 s) and an average NL of the amplitude ratios of 0.05 +/− 0.10. The highly confined ray paths are centered beneath (0°, 30° E).

Results

In general, the differential times (O-C) of PKiKP-PKIKP show some resemblance to the quasi-hemispherical pattern (Fig. 3), but important differences can be also noticed. Recordings of Banda Sea (or Java) events at stations in the NE Canada and United States systematically show differential PKIKP/PKiKP times around −0.2 seconds, despite the corresponding rays sample the qEH beneath the Northern Pacific, Siberia or Central part of Northern Eurasia. The same situation is seen for the earthquakes in South Pacific (e.g. Papua New Guinea) observed at stations in Spain/Portugal, for most of the Vanuatu events observed at stations in Israel or Turkey, or for the Solomon Islands earthquakes observed in Germany and France. Such observations do not support the quasi-hemispherical dichotomy of the IC with a certain longitude line separation, at least along 180° meridian.

There are no areas in Fig. 3 showing a large number of rays at a broad range of orientations to display a pattern reliably suggesting the presence of anisotropy at large scales. Most of Eastern Asia is highly sampled by 245 core phases from 25 Vanuatu events recorded by various stations located in Egypt, Israel, Turkey and Europe. Most of the corresponding differential times are close to zero (around −0.1 to −0.2 seconds). There is no pattern suggesting the presence of anisotropy here, in spite of the broad ray orientations, from a near equatorial one (when sampling IC beneath Indochina) to a near polar path (beneath Kamchatka). The rays sampling the IC beneath Australia and surrounding areas are oriented both on a North-South direction and parallel to the Equator. Yet, all the corresponding differential times are close to zero. They suggest the absence of UIC anisotropy here[30]. Beneath the North Pacific, there are rays with both near equatorial and near polar paths, but all the differential times show slightly negative values. The last observation suggests not only the lack of anisotropy here, but also the absence of a q-H separation at high latitudes around 180° meridian.

A more complex pattern is seen beneath South Africa. In the framework of a q-H IC, such observations have been considered as a result of a complex IC, displaying important vertical and horizontal perturbations in the (isotropic) velocity, anisotropy and attenuation[9,10]. However, rays at different orientations do not sample exactly the same volume of the IC. There are basically two orientations only, a quasi-equatorial and a quasi-polar one. While many quasi-polar observations (of higher quality) are available, there are only a limited number of equatorial ones (of low to moderate quality). It is difficult to accurately estimate here the three parameters describing the anisotropy.

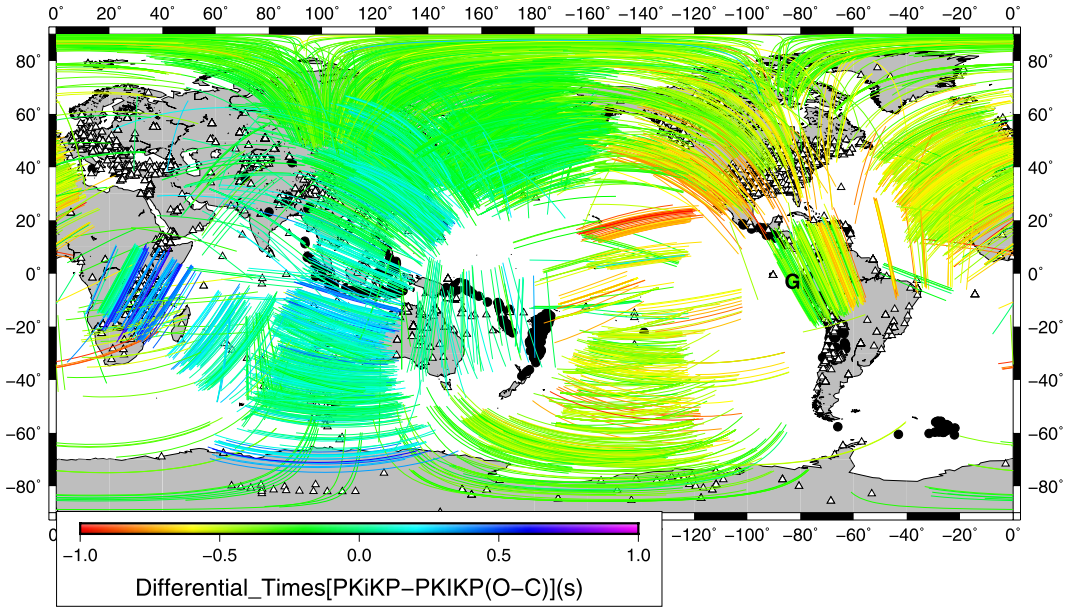

Figure 3. Differential times of PKiKP-PKIKP (O-C) observations. Triangles indicate the seismological stations and black filled circles are the epicenters. Colored lines correspond to the PKIKP paths into the inner core. Pont G at (0°, 80°W) is indicated. Figure produced with Generic Mapping Tools (GMT 5.1.2)[48].

A similar situation is observed beneath the Northern part of the Southern America, where all the observations are near polar ones, showing a regional horizontal gradient in the differential times[31]. Consequently, it is hard to discriminate here between anisotropy and heterogeneity too[32].

Inversion Results and Discussion

For a station at 138° distance, both PKIKP and PKiKP at 1 Hz have the Fresnel diameter along ICB around 19°. At the PKIKP ray turning point, the vertical Fresnel diameter exceeds 250 km[33]. The ability of PKIKP to resolve structures at a scale much below the above values, both horizontally and vertically, is questionable. The use of the synthetic seismograms obtained with 1-D model in such complex areas is problematic too, especially when the ray turning point is considered as being representative for the whole ray path of PKIKP in the IC. For a PKIKP recorded at 138 degrees, the last approach may introduce its own errors in the location of the velocity perturbation as large as 16 degrees in the horizontal direction.

Consequently, we prefer to interpret the differential time values as a result of heterogeneity rather than of anisotropy, without excluding that anisotropy could be present in some restricted areas. We divide each of the two uppermost layers of the IC in the ak135 model into cells of $20° \times 20°$ degrees. The travel time corresponding to the IC leg of PKIKP is around 65 seconds and the observed differential times are in the range −1.0 to 0.7 seconds. So, we invert the differential times assuming that the isotropic velocity perturbations are in the range −1.2 to 1.2%. The inversion results are interpolated by kriging method with low smoothing[34]. Such an approach is more able to preserve the strong lateral gradients[35], if existing in the UIC structure. However, it is also expected to produce some small, detailed patches not necessary entirely supported by the input data, which are routinely removed by various interpolation methods and/or supplemental filtering[36]. A checkerboard test shows good resolution results (see Figures S1, S2 in the Supplemental Material), especially for the cells hit by more than 43 rays (around 5% of the maximum number of rays crossing a cell, which is 862). The differential time values are explained as a result of velocity perturbations along the whole path of PKIKP in the IC. Inversion is done for the two vertical layers above only to seek consistency with the ak135 model, thoroughly used in this study. So, any significant vertical variations of velocity perturbation obtained between the two layers in our inversion should be regarded with care, given the Fresnel diameter of PKIKP.

The inversion results explain more than 80% of the data variance. They show that UIC is mainly represented by a low velocity cap (Fig. 4 and Supplemental Fig. S3) extended beneath most of the so-called qWH, but also beneath the northern part of Eurasia. A local maximum around (0°, 90°W) is mainly the result of a north-northeast to south-southwest gradient in the observed differential times. A similar pattern has been observed in the same area for PKiKP vs. PcP amplitudes (the last phase is the P wave reflected by the core-mantle boundary). This has been explained by a patch of mushy material of a few kilometers high, with a gradual change from the outer core to the IC[37]. This could also explain the extinction (very low amplitudes) of PKiKP bouncing ICB in that area, for some of the South Sandwich events recorded by the Canadian stations (Supplemental Fig. S4).

The rest of the UIC, which is more heterogeneous, is mainly represented by a higher velocity cap with a radius around 60°, roughly centered beneath the northern Sumatra. There are several local maxima here. The first one, placed beneath Sumatra, is the result of south Pacific events observed at the African stations. A second one is located beneath the southeast Africa (0°, 30°E), probably extended toward the southern part of the Indian Ocean.

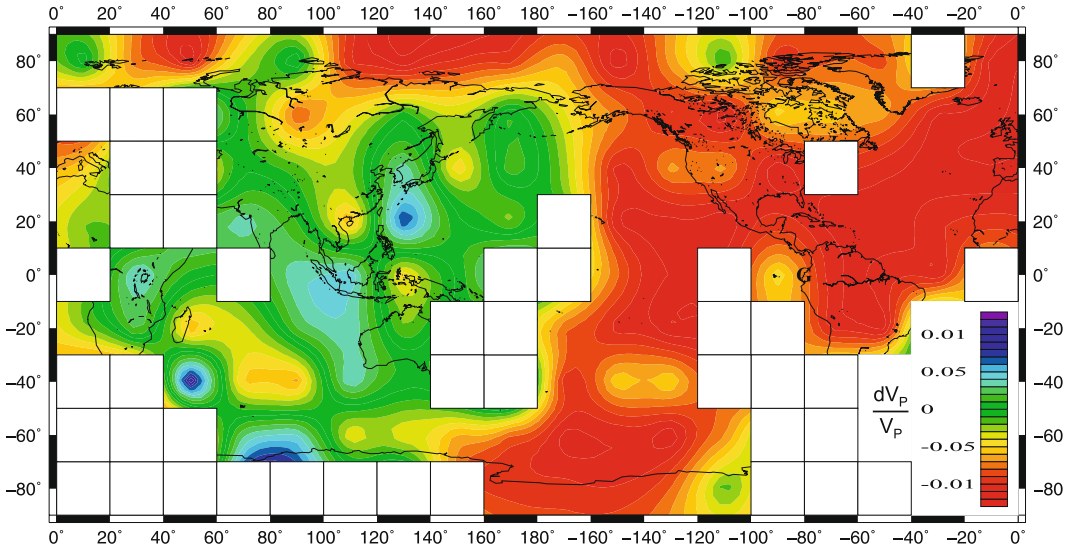

Figure 4. Velocity perturbations at the top of the inner core (first layer beneath ICB in ak135 model, depth from 0 to 51.11 km beneath ICB). Data have been interpolated with kriging method[34] and a low smoothing. White squares show the areas where the small number of rays did not allow reliable results. The model explains more than 80% in the initial variance (evaluated for null velocity perturbations). Point G at (0°, 80°W) is indicated. Figure produced with Generic Mapping Tools (GMT 5.1.2)[48].

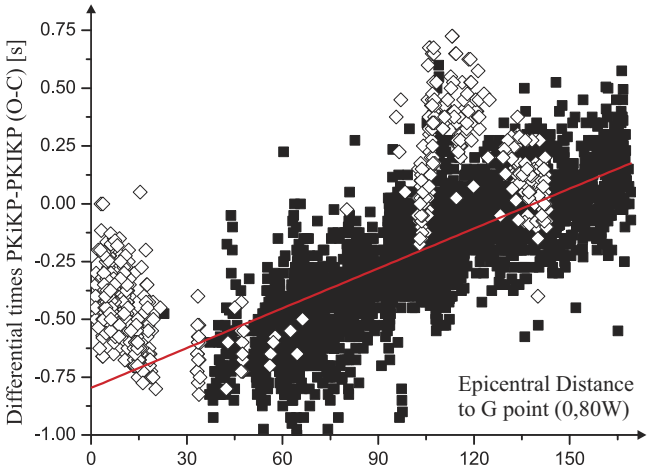

Figure 5. Differential times PKiKP-PKIKP vs. angular distance of the PKIKP bouncing point to the (growth) G point (0, 80°W). Significant departures from the regression line can be observed near 15° or 120° distances due to some of the observations related mainly to some South Sandwich earthquakes (white diamonds). R-square value is 0.58.

It is mainly the consequence of various observations of South Sandwich events recorded by Central Asian stations. The local maximum around (20°N, 130°E) is suggested by various recordings at European stations of the South Pacific earthquakes. Other local maxima around (0, 90°W) and (40°S, 140°W) are well supported too by the corresponding differential times observations. A low velocity area is observed beneath the central Indian Ocean around (40°S, 80°E), likely to be extended towards NorthWest, in agreement with other previous observations[38]. Irrespective the checkerboard test results, we estimate the rest of the small patches are less supported, being most likely a result of the adopted parametrization and, especially, of the kriging interpolation with low filtering.

There are a few negative differential times in Fig. 3 for rays beneath southwest Africa, observed for some Sandwich events recorded at the Asian stations. The number of rays crossing this area is too small to allow a definite conclusion. A low-velocity volume in the UIC beneath southernmost Africa could be an alternative possible explanation to the anisotropy in that region[9], suggesting the presence of a convective cell here[16], could be correlated with an anomalous low-velocity zone near core-mantle boundary, present in various tomographic models[39–41].

Given the above comments about the Fresnel zone, we also use a single-layer (~100 km thick) model in inversion. The results (Supplemental Figures S5 and S6) are quite similar to the one obtained for the two-layers

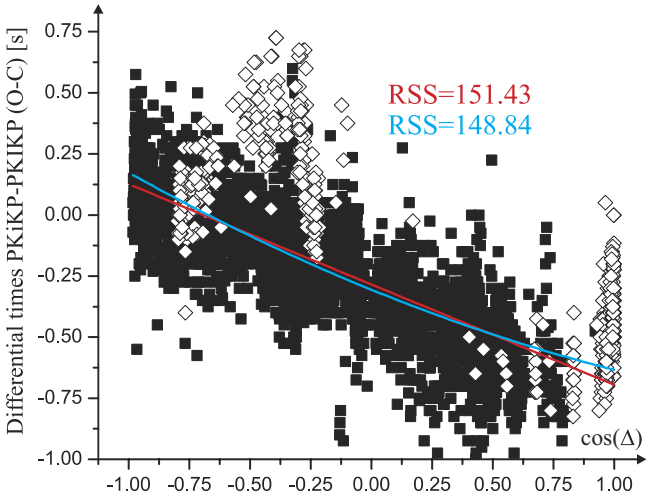

Figure 6. Differential times PKiKP-PKIKP vs. cosine of the angular distance of the PKIKP bouncing point to the (growth) G point (0, 80°W). The values of the Residual sum of Squares are indicated both for the linear (red, degree one spherical harmonic pattern, SHP) and the second order fit (blue, degree two SHP). The Akaike Criterion[42] is minimized by the quadratic fit in respect to the linear fit.

inversion. All of them suggest the low velocity zone beneath Central Indian Ocean and the local maximum around (0°, 90°W) have a limitted extend in depth beneath the IC boundary.

We also investigated the possible degree one hemispherical pattern of the differential times considering the distance Δ to an equatorial pole located at 80°W[12]. Figure 5 shows the observations that provide limited support for such a model. The R-squared value obtained for a linear fit in Δ is increased by only 9% when the observations are fitted by a linear model in cos(Δ) (Fig. 6). According to a criterion from the information theory[42], a better fit is represented by a degree two polynomial (in cos(Δ)). However, significant departures from a theoretical linear (or degree two) pattern are observed again near distances of 15° and 120°, especially due to some (but not all) of the South Sandwich events recordings.

Conclusions

The spatial distribution of heterogeneity in the UIC shows important differences relative to the rest of the IC. It is commonly assumed that the former shows not only a quasi-hemispherical pattern, with a separation along certain meridians, but also anisotropy, with a north-south fast axis[43–45].

The presence of two maxima (beneath Sumatra snd the south-eastern Africa) can be better explained by thermal models which allow a more complex pattern of the temperatures near ICB[16]. Our seismological observations provide important constraints to the mantle and core convection, leading to a better understanding of the Earth's dynamo.

Neither the observed differential times nor the results of the inversion support a sharp boundary of the higher velocity cap, at least beneath the northern part of Eurasia.

There is a large variance of the amplitude ratio observations, suggesting a weak (if any) correlation between regions with higher velocity and lower attenuation in the UIC. It may support the possible presence of a mushy zone, or a mosaic-like ICB[46,47]. It may be also the effect of very short-scale heterogeneities (~75 km length) located near core-mantle boundary. The amplitude ratio of the high signal to noise recordings of the South Sandwich events observed at the Central Asia stations does not support models asking for a substantial change of the Q attenuation factor in the UIC in respect to ak135 model' at least around (0°, 30° E)[48].

References

1. Alboussière, T., Deguen, R. & Melzani, M. Melting-induced stratification above the Earth's inner core due to convective translation. *Nature* **466**, 744–747 (2010).
2. Tkalčić, H. *Inner Core Surface and Its Interios in The Earth's Inner Core* 38–73 (Cambridge, 2017).
3. Niu, F. & Wen, L. Hemispherical variations in the seismic velocity at the top of the Earth's inner core. *Nature* **410**, 1081–1084 (2001).
4. Irving, J. C. E. & Deuss, A. Hemispherical structure in inner core velocity anisotropy. *J. Geophys. Res.* **116**, B04307 (2011).
5. Yee, T.-G., Rhie, J., & Tkalčić, H. Regionally heterogeneous uppermost inner core observed with Hi-net array. *J. Geophys. Res.* https://doi.org/10.1002/2014JB011341 (2014).
6. Shearer, P. M. Constraints on inner core anisotropy from PKP(DF) travel times. *J. Geophys. Res.* **99**(19), 647–19,659 (1994).
7. Song, X. D. & Helmberger, D. V. Depth dependency of anisotropy of Earth's inner core. *J. Geophys. Res.* **100**, 9805–9816 (1995).
8. Song, X. & Helmberger, D. V. Seismic evidence for an inner core transition zone. *Science* **282**, 924–927 (1998).
9. Yu, W. & Wen, L. Complex seismic anisotropy in the top of the Earth's inner core beneath Africa. *J. Geophys. Res.* **112**, B08304, https://doi.org/10.1029/2006JB004868 (2007).
10. Waszek, L., Irving, J. & Deuss, A. Reconciling the hemispherical structure of the Earth's inner core with its super-rotation. *Nat. Geosci.*. https://doi.org/10.1038/NGEO1083 (2011).
11. Yu, W. *et al*. The inner core hemispheric boundary near 180 °W. *Phys. Earth Planet. Inter*. https://doi.org/10.1016/j.pepi.2017.09.002 (2017).
12. Monnereau, M., Calvet, M., Margerin, M. & Souriau, A. Lopsided growth of Earth's inner core. *Science* **328**, 1014–1017 (2010).

13. Dai, Z., Wang, W. & Wen, L. Irregular topography at the Earth's inner core boundary. *PNAS* **109**, 7654–7658 (2012).
14. Cormier, V. F. & Attanayake, J. Earth's Solid Inner Core: Seismic Implications of Freezing and Melting. *J. Earth Sci.* **24**(5), 683–698, https://doi.org/10.1007/s12583-013-0363-9 (2013).
15. Aubert, J., Amit, H., Hulot, G. & Olson, P. Thermochemical flows couple the Earth's inner core growth to mantle heterogeneity. *Nature* **454**, 758–761, https://doi.org/10.1038/nature07109 (2008).
16. Gubbins, D., Sreenivasan, B., Mound, J. & Rost, S. Melting of the Earth's Inner Core. *Nature* **473**, 361–363 (2011).
17. Waszek, L. & Deuss, A. Distinct layering in the hemispherical seismic velocity structure of Earth's upper inner core. *J. Geophys. Res.* **116**(B12), 313, https://doi.org/10.1029/2011JB008650 (2011).
18. Geballe, Z. M., Lasbleis, M., Cormier, V. F. & Day, E. A. Sharp hemisphere boundaries in a translating inner core. *Geophys. Res. Lett.* **40**, 1–5, https://doi.org/10.1002/grl.50372 (2013).
19. Ohtaki, T., Kaneshima, S. & Kanjo, K. Seismic structure near the inner core boundary in the South Polar Region. *J. Geophys. Res.* **117**, B03312, https://doi.org/10.1029/2011JB008717 (2012).
20. Krasnoshchekov, D., Kaazik, P., Kozlovskaya, E. & Ovtchinnikov, V. Seismic structures in the Earth's inner core below Southeastern Asia. *Pure Appl. Geophys.* **173**, 1575–1591 (2016).
21. Iritani, R., Takeuchi, N. & Kawakatsu, H. Intricate heterogeneous structures of the top 300 km of the Earth's inner core inferred from global array data: I. Regional 1D attenuation and velocity profiles. *Phys. Earth Planet. Inter.* **230**, 15–27 (2014).
22. Miller, M. S., Niu, F. & Vanacore, E. A. Aspherical structural heterogeneity within the uppermost inner core: Insights into the hemispherical boundaries and core formation. *Phys. Earth Planet. Inter.* **223**, 8–20 (2013).
23. Irving, J. C. E. & Deuss, A. Regional seismic variations in the inner core under the North Pacific. *Geophys. J. Int.* **203**, 2189–2199 (2015).
24. Wang, R., Heimann, S., Zhang, Y., Wang, H., & Dahm, T. Complete synthetic seismograms based on a spherical self-gravitating Earth model with an atmosphere-ocean-mantle-core structure. *Geophys. J. Int.* https://doi.org/10.1093/gji/ggx259 (2017).
25. Dziewonski, A. M., Chou, T.-A. & Woodhouse, J. H. Determination of earthquake source parameters from waveform data for studies of global and regional seismicity. *J. Geophys. Res.* **86**, 2825–2852 (1981).
26. Ekström, G., Nettles, M. & Dziewonski, A. M. The global CMT project 2004–2010: Centroid-moment tensors for 13,017 earthquakes. *Phys. Earth Planet. Inter.* **200–201**, 1–9, https://doi.org/10.1016/j.pepi.2012.04.002 (2012).
27. Engdahl, E. R. & Gunst, R. H. Use of a high speed computer for the preliminary determination of earthquake hypocenters. *Bull. Seismol. Soc. Am.* **56**, 325–336 (1966).
28. International Seismological Centre. On-line Bulletin http://www.isc.ac.uk. Thatcham: International Seismological Centre (2013).
29. Cao, A. & Romanowicz, B. Hemispherical transition of seismic attenuation at the top of the Earth's inner core. *Earth Planet. Sci. Lett.* **228**, 243–253 (2004).
30. Isse, T. & Nakanishi, I. Inner-core anisotropy beneath Australia and differential rotation. *Geophys. J. Int.* **151**, 255–263 (2002).
31. Creager, K. C. Inner core rotation rate from small-scale heterogeneity and time-varying travel times. *Science* **278**, 1284–1288 (1997).
32. Blom, N. A., Deuss, A., Paulssen, H. & Waszek, L. Inner core structure behind the PKP core phase triplication. *Geophys. J. Int.* **201**, 1657–1665 (2015).
33. Kvasnička, M. & Janský, J. Fresnel volumes corresponding to PKP waves in the IASP91 model. *J. Seismol.* **3**, 375–391 (1999).
34. Watson, G. S. Smoothing and interpolation by kriging and with splines. *Math. Geol.* **16**, 601–616 (1984).
35. Tkalčić, H., Romanowicz, B. & Houy, N. Constraints on D structure using PKP(AB–DF), PKP(BC–DF) and PcP–P traveltime data from broad-band records. *Geophys. J. Int.* **148**, 599–616 (2002).
36. Nolet, G. *A Breviary of Seismic Tomography*, Cambridge, (2008).
37. Li, D., Sun, D. & Helmberger, D. Notes on the variability of reflected inner core phases. *Earthq. Sci.* **27**(4), 441–468, https://doi.org/10.1007/s11589-014-0093-9 (2014).
38. Stroujkova, A. & Cormier, V. F. Regional variations in the uppermost 100 km of the Earth's inner core. *J. Geophys. Res.* **102**, 2925–2938 (2004).
39. Obayashi, M. *et al*. Finite frequency whole mantle P wave tomography: Improvement of subducted slab images. *Geophys. Res. Lett.* **40**, 5652–5657, https://doi.org/10.1002/2013GL057401 (2013).
40. Fukao, Y. & Obayashi, M. Subducted slabs stagnant above, penetrating through, and trapped below the 660 km discontinuity. *J. Geophys. Res.* **118**, 5920–5938, https://doi.org/10.1002/2013JB010466 (2013).
41. Simmons, N. A., Myers, S. C., Johannesson, G. & Matzel, E. LLNL-G3Dv3: Global P wave tomography model for improved regional and teleseismic travel time prediction. *J. Geophys. Res.* **117**, B10302, https://doi.org/10.1029/2012JB009525 (2012).
42. Akaike, H. Information theory and an extension of the maximum likelihood principle, In Petrov, B. N.; Csáki, F., 2nd International Symposium on Information Theory, Tsahkadsor, Armenia, USSR, September 2–8, 1971, Budapest: Akadémiai Kiadó, 267–281 (1973).
43. Morelli, A., Dziewonski, A. M., & Woodhouse, J. H. Anisotropy of the core inferred from PKIKP travel times. *Geophys. Res. Lett.* https://doi.org/10.1029/GL013i013p01545 (1986).
44. Tanaka, S. & Hamaguchi, H. Degree one heterogeneity and hemispherical variation of anisotropy in the inner core from PKP (BC)–PKP (DF) times. *J. Geophys.Res.* **102**, 2925–2938 (1997).
45. Song, X. Anisotropy of the Earth's inner core. *Rev. Geophys.* **35**, https://doi.org/10.1029/97RG01285 (1997).
46. Krasnoshchekov, D. N., Kaazik, P. B. & Ovtchinnikov, V. M. Seismological evidence for mosaic structure of the surface of the Earth's inner core. *Nature* **435**, 483–487 (2005).
47. Loper, D. E. & Roberts, P. H. A study of conditions at the inner core boundary of the Earth. *Phys. Earth Planet. Inter.* **24**, 302–307 (1981).
48. Wessel, P. & Smith, W. H. F. A global, self-consistent, hierarchical, high-resolution shoreline database. *J.Geophys. Res.* **104**, 4795–4809 (1996).
49. Garcia, R. Constraints on upper inner-core structure from waveform inversion of core phases. *Geophys. J. Int.* **150**, 651–664 (2002).

Acknowledgements

We thank to various Data Centers that contributed waveforms (IRIS, ORFEUS-EIDA, F-net, Canadian DC, German SZGRF, Israel and Romania national networks). Some figures have been produced with the Generic Mapping Tools (GMT 5.1.2).

Author Contributions

R.W. wrote the QSSP code to compute synthetics (freely available for download at ftp://ftp.gfz-potsdam.de/pub/home/turk/wang/qssp2010-code+input.rar) and provided input files for computing synthetics. R.H. contributed to data acquisition and preliminary data processing. M.I. took the lead in writing the manuscript, performed the main analysis and wrote the rest of the codes. All authors contributed to the final version of the manuscript.

Additional Information

Supplementary information accompanies this paper at https://doi.org/10.1038/s41598-018-20657-x.

Competing Interests: The authors declare that they have no competing interests.

Publisher's note: Springer Nature remains neutral with regard to jurisdictional claims in published maps and institutional affiliations.

Open Access This article is licensed under a Creative Commons Attribution 4.0 International License, which permits use, sharing, adaptation, distribution and reproduction in any medium or format, as long as you give appropriate credit to the original author(s) and the source, provide a link to the Creative Commons license, and indicate if changes were made. The images or other third party material in this article are included in the article's Creative Commons license, unless indicated otherwise in a credit line to the material. If material is not included in the article's Creative Commons license and your intended use is not permitted by statutory regulation or exceeds the permitted use, you will need to obtain permission directly from the copyright holder. To view a copy of this license, visit http://creativecommons.org/licenses/by/4.0/.

© The Author(s) 2018